PLOS ONE

RESEARCH ARTICLE

A mathematical model of aortic aneurysm formation

Wenrui Hao[1]*, Shihua Gong[2], Shuonan Wu[1], Jinchao Xu[1], Michael R. Go[3], Avner Friedman[4], Dai Zhu[5]

1 Department of Mathematics, Pennsylvania State University, State College, PA, United States of America, **2** Beijing International Center for Mathematical Research, Peking University, Beijing, China, **3** Division of Vascular Diseases & Surgery, The Ohio State University Wexner Medical Center, Columbus, OH, United States of America, **4** Department of Mathematics, The Ohio State University, Columbus, OH, United States of America, **5** Yunnan Cocreative Scientific Computing and Datamining Center, Kunming, China

* wxh64@psu.edu

Citation: Hao W, Gong S, Wu S, Xu J, Go MR, Friedman A, et al. (2017) A mathematical model of aortic aneurysm formation. PLoS ONE 12(2): e0170807. doi:10.1371/journal.pone.0170807

Editor: Luigi F. Rodella, University of Brescia, ITALY

Received: April 28, 2016

Accepted: January 11, 2017

Published: February 17, 2017

Data Availability Statement: All relevant data are within the paper.

Funding: WH was a postdoctoral researcher at Mathematical Biosciences Institute at the time of the study and received financial support from the institution. WH and AF received funding from the National Science Foundation under Grant 0931642. The funders had no role in study design, data collection and analysis, decision to publish, or preparation of the manuscript.

Competing interests: The authors have declared that no competing interests exist.

Abstract

Abdominal aortic aneurysm (AAA) is a localized enlargement of the abdominal aorta, such that the diameter exceeds 3 cm. The natural history of AAA is progressive growth leading to rupture, an event that carries up to 90% risk of mortality. Hence there is a need to predict the growth of the diameter of the aorta based on the diameter of a patient's aneurysm at initial screening and aided by non-invasive biomarkers. IL-6 is overexpressed in AAA and was suggested as a prognostic marker for the risk in AAA. The present paper develops a mathematical model which relates the growth of the abdominal aorta to the serum concentration of IL-6. Given the initial diameter of the aorta and the serum concentration of IL-6, the model predicts the growth of the diameter at subsequent times. Such a prediction can provide guidance to how closely the patient's abdominal aorta should be monitored. The mathematical model is represented by a system of partial differential equations taking place in the aortic wall, where the media is assumed to have the constituency of an hyperelastic material.

Introduction

AAA is an abnormal dilatation most commonly of the infrarenal aorta. One definition of AAA is a diameter greater than 3 cm [1]. The clinical significance of AAA stems from the high mortality associated with rupture. Approximately 60% of patients with ruptured AAA die before reaching the hospital [2] and mortality rates of emergency surgical repair are as high as 35–70% [3]. The risk of rupture increases with AAA diameter. The pathogenesis of AAA is largely unknown and likely multifactorial. Diameter remains the only clinically useful and available marker for risk of rupture. Surgical repair is recommended for aneurysms measuring greater than 5.5 cm [4, 5] and there is insufficient evidence to recommend surgery for all patients with smaller AAA [2]. However, even elective surgical repair of AAA remains a major operation, incurring significant morbidity and mortality particularly in older, sicker patients where there is a higher prevalence of AAA. Furthermore, patients die every year from rupture of aneurysms smaller than 5.5 cm, and up to 60% of AAA larger than 5 cm remain stable [6]. Thus,

some patients with smaller AAA are denied lifesaving surgery and others with larger AAA undergo unnecessary major surgery. The reasons why some smaller aneurysms go on to rupture while some larger ones remain stable are not understood. Techniques that provide early identification of small AAA with increased risk for rupture and large AAA with low risk for rupture will improve overall mortality by prompting personalized treatment plans for AAA.

There are a number of mathematical papers that describe the dynamics of the weakening and dilation of the arterial wall and the risk of rupture. The more comprehensive models include the nonlocal, nonlinear elastic nature of the arterial wall in response to wall shear stress [7–10]. However these models do not explain the clinical fact that some abdominal aortae rupture when the diameter of the cross section of the dilated aorta is less than 5.5 cm while others do not rupture even when much larger than 5.5 cm. There is a need to discover non-invasive biomarkers that will provide the following prognosis for a patient undergoing initial screening for AAA:

- Given initial diameter of the cross section of the aorta, say R_0, how will the diameter, say $R(t)$, evolve with time?
- How will the risk of rupture increase with time?

The present paper develops a mathematical model that addresses the first question, with IL-6 as the serum biomarker. IL-6 has already been suggested as prognostic biomarker for AAA in [11, 12]; additional potential biomarkers are reviewed in [13, 14].

The mathematical model consists of two parts. The first part focuses on the biology. It introduces a network of cells and cytokines which, in disease state, lead to the destruction of smooth muscle cells (SMCs) and elastin depletion in the media, and disruption of the extracellular matrix (ECM) in the adventitia. The biological predictions of this part of the model, in terms of the expression levels of the proteins involved, are in agreement with patients data [15]. The second part of the model develops the mechanics of diameter growth of the artery as a result of deficiency in elastin and disruptions in the ECM. Here, instead of the approach taken in [7–10], we use the fact that the arterial wall behaves like a hyperelastic material [16]. Hence its elastic strength and displacement under stress depend on the smooth muscle cells in the aortic wall. We can therefore relate the wall dilation to several cytokines whose expression is upregulated in disease state. Such cytokines could be used as potential biomarkers for predicting the arterial wall dilation. We shall focus on IL-6, which is upregulated in AAA patients [11, 12].

The biological network introduced in the present paper includes macrophages, T cells, SMCs and fibroblasts, as well as cytokines such as IL-6, IL-10, IL-12, TNF-α and IFN-γ; MMP and TIMP are also included. The densities of the cells and the concentrations of the proteins satisfy a coupled system of partial differential equations (PDEs) in the arterial wall.

In the early stage of aneurysm, endothelial cells, under hemodynamic shear stress, secrete major attractant protein, MCP-1, and IL-6 [17]. IL-6 is also produced by SMCs (in conjunction with IL-1) [18]. This triggers recruitment of monocytes from the blood into the media layer of the arterial wall [19]. The monocytes mature into macrophages, while, at the same time, additional macrophages from the adventitia are also chemoattracted by MCP-1, IL-6 and IL-8 [20–22]. More precisely, IL6/MCP-1 combined, and MCP-1 and IL-8 separately chemoattract monocytes; for simplicity, we shall represent the chemoattractants by MCP-1 and IL-6. T cells are activated by contact with macrophages in the presence of IL-12, and macrophages are activated by IFN-γ produced by the T cells [23]. Macrophages produce TNF-α [24], MMP and TIMP [24, 25], and IL-10, IL-12 and IL-6 [26], but MMP is also produced by SMCs [27]. Fibroblasts produce collagen [28], and the collection of MMP, TIMP and collagen weaken the ability

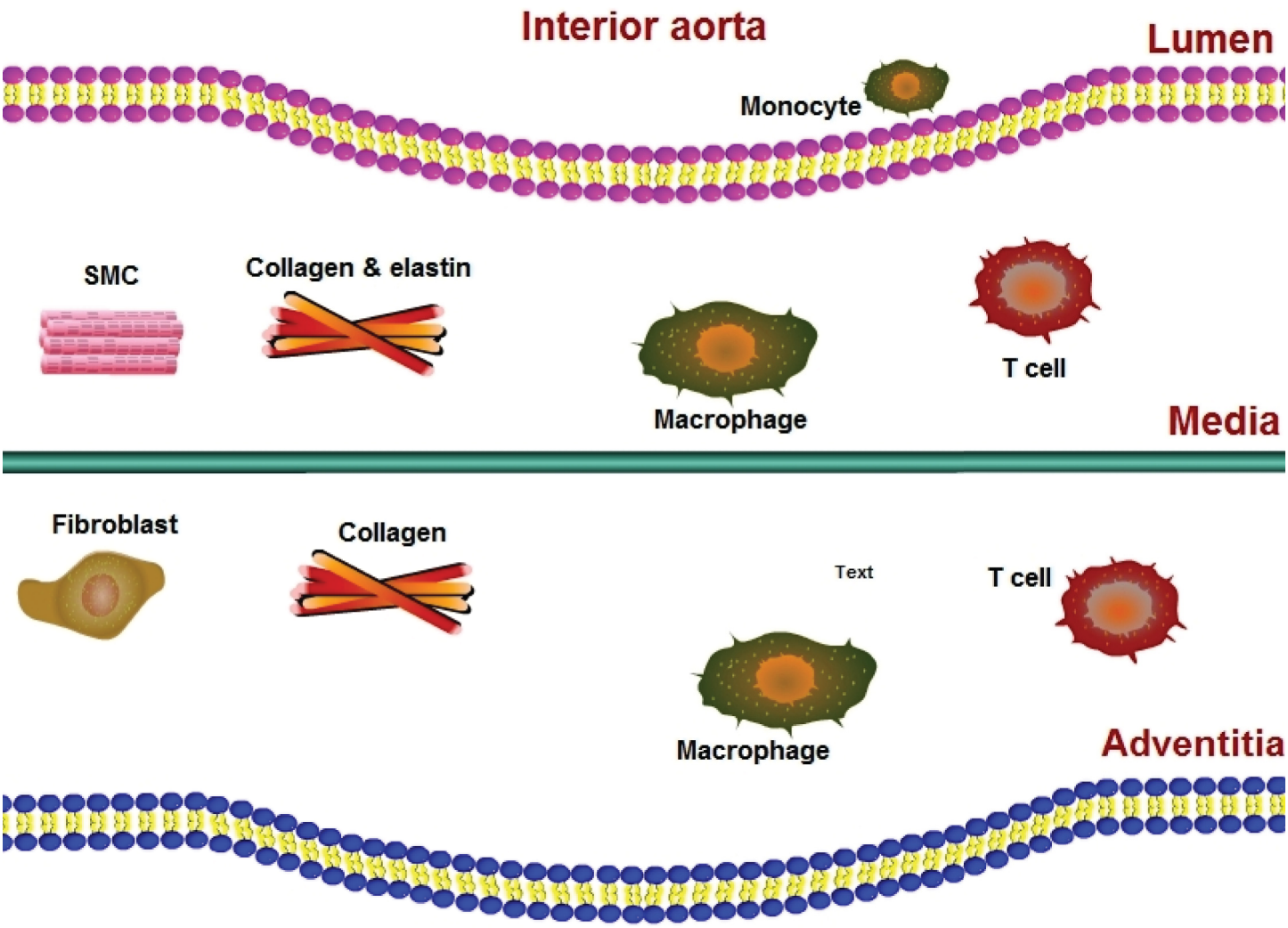

Fig 1. A schematic of the aortic wall including the aortic lumen, the intima, media, and adventitia.

doi:10.1371/journal.pone.0170807.g001

of the adventitia layer to withstand stress. Macrophages are known to cause apoptosis in SMCs [19], and this leads to reduction in elastin [29], thus weakening the elastic strength of the media; The apoptotic SMCs are known to produce MCP-1 [19].

Fig 1 shows SMCs residing in the media, fibroblasts residing in the adventitia, while macrophages and T cells are present in both layers of the aortic wall.

Fig 2 is a schematics of the network within the arterial wall during aneurysm; all the cytokines and the ECM (elastin and collagen) are present in both the media and the adventitia. A schematics of the balloon-like bulge geometry in the aorta is shown in Fig 3.

1 Mathematical model of the biology

In this section we develop a mathematical model of aneurysm based on the diagram shown in Fig 2. The model, represented by a system of PDEs, includes the variables listed in Table 1. We assume that all cells are moving with a common velocity **v**; the velocity is the result of movement of macrophages, T cells and SMCs into the media and adventitia. We also assume that all

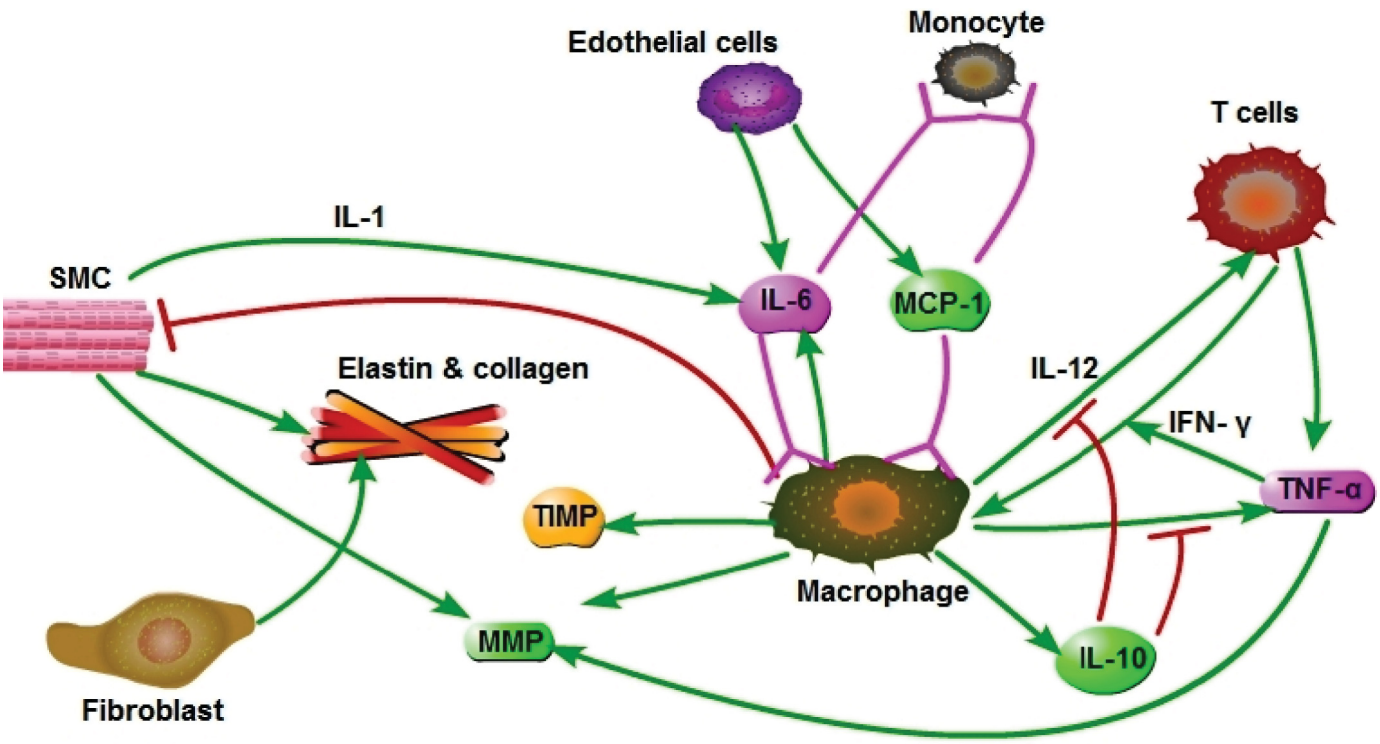

Fig 2. Interaction network among cells and cytokines in their respective layers. SMCs remain in the media, and fibroblasts remain in the adventitia.

doi:10.1371/journal.pone.0170807.g002

species are diffusing with appropriate diffusion coefficients. The equation for each species of cells, X, has a form

$$\frac{dX}{dt} + \nabla \cdot (\mathbf{v}X) - D_X \Delta X = F_X,$$

where the expression on the left-hand side includes advection and diffusion, and F_X accounts for various biochemical reactions, and chemotaxis. The equations for the chemical species are the same as for cells, but without the advection term, which is relatively very small compared to their large diffusion coefficients. Fig 3 shows a 2D projection of a blood vessel Ω_B with an aortic aneurysm $\Omega_M \cup \Omega_A$.

Equation for MCP-1 (P)

The equation for MCP-1 is given in the whole domain (media Ω_M, and adventitia Ω_A) by

$$\frac{\partial P}{\partial t} - D_P \Delta P = \underbrace{\lambda_{PS} \frac{M}{M + K_M} S}_{production} \underbrace{- d_{PM} \frac{P}{P + K_P} M - d_P P}_{degradation}, \quad (1)$$

The first term on the right-hand side is the production of P by apoptotic SMCs, which is induced by macrophages [19]. The second term represents lost of MCP-1 as it binds to, and internalized by, macrophages which are chemoattracted to MCP-1; the internalization of MCP-1 may be limited due to the limited rate of receptor recycling. The last term in Eq (1) accounts for degradation of MCP-1.

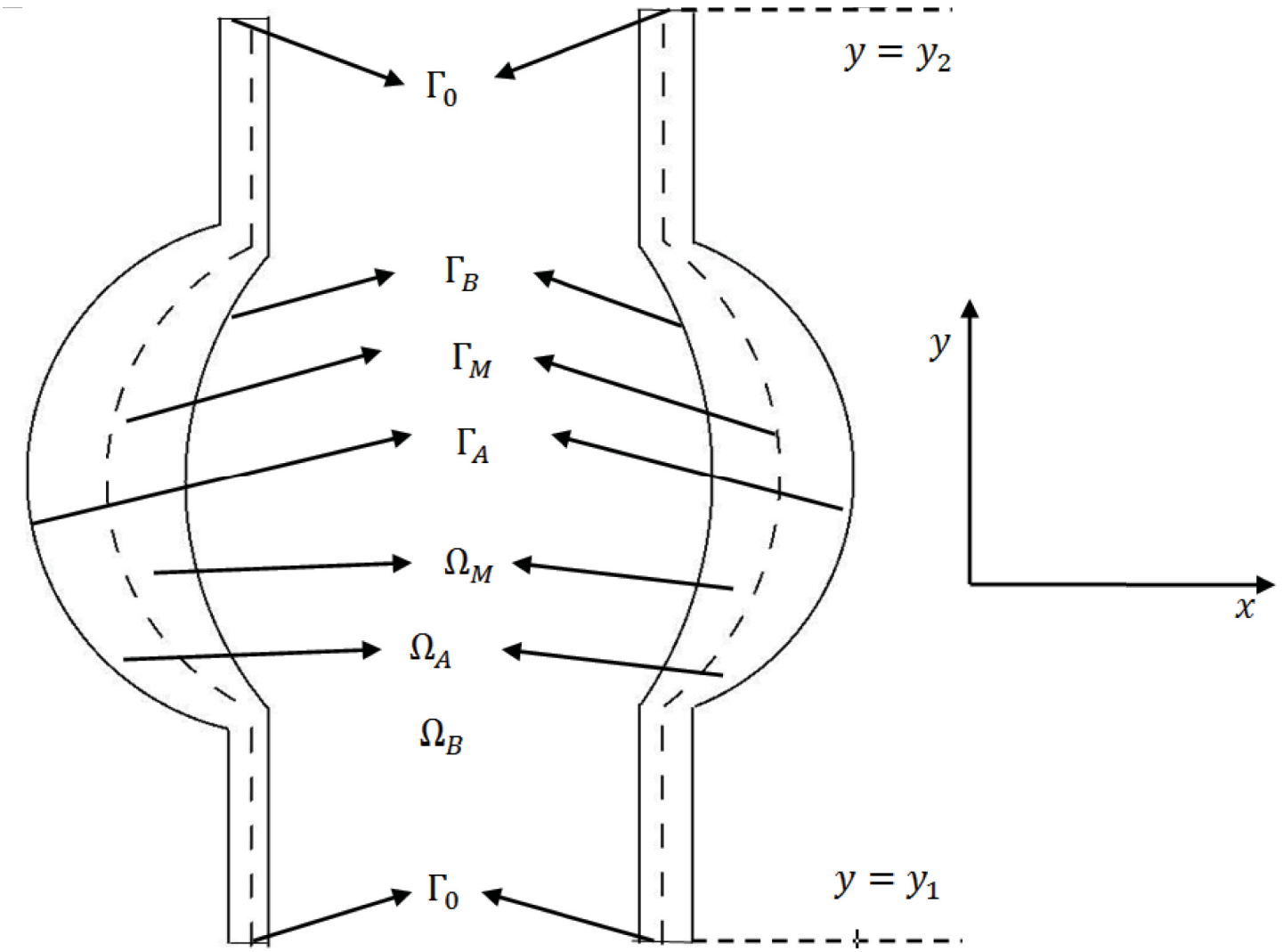

Fig 3. Schematic representation of a 2D section of the computational domain. Ω_B is blood vessel; Ω_M represents the media and Ω_A the adventitia; Γ_A, Γ_B and Γ_M are three free boundaries. Γ_B is the inner surface of the artery, Γ_A is the outer surface, and Γ_M is the surface between the media and adventitia.

doi:10.1371/journal.pone.0170807.g003

Table 1. The variables of the model; concentration and densities are in units of g/cm^3.

S:	density of SMCs	T:	density of T cells (Th1)
M:	density of macrophages	f:	density of fibroblasts
ρ:	density of ECM	P:	concentration of MCP-1
T_α:	concentration of TNF-α	I_γ:	concentration of INF-γ
I_6:	concentration of IL-6	I_{10}:	concentration of IL-10
I_{12}:	concentration of IL-12	Q:	concentration of MMPs
Q_r:	concentration of TIMP	p:	pressure in media (in $g/cm/day^2$)
u:	displacement (in *cm*)	**v**:	cell velocity in media and adventitia (in *cm*/*day*)

doi:10.1371/journal.pone.0170807.t001

Equation for macrophages (M)

According to [26] the two phenotype of macrophages, M1 and M2, are both present in aneurysm; M1 secretes inflammatory cytokines such as IL-12 and TNF-α, while M2 secretes immunoregulatory cytokines such as IL-10. For simplicity, we do not differentiate between the two phenotypes, but take into account that the productions of IL-12 and TNF-α are resisted by IL-10 [30].

The evolution of the macrophage density in $\Omega_M \cup \Omega_A$ is modeled by

$$\begin{aligned} \frac{\partial M}{\partial t} + \nabla \cdot (\mathbf{v}M) - D_M \Delta M &= \underbrace{-\nabla \cdot (M\chi_C \nabla P) - \nabla \cdot (M\chi_C \nabla I_6)}_{chemotaxis} \\ &\quad \underbrace{+\lambda_{ML_\gamma} M \frac{I_\gamma}{I_\gamma + K_{I_\gamma}} \left(1 + \lambda_{MT_\alpha} \frac{T_\alpha}{T_\alpha + K_{T_\alpha}}\right)}_{activation} \underbrace{-d_M M}_{death}. \end{aligned} \tag{2}$$

The first two terms on right-hand side account for the recruitment of macrophages by MCP-1 [19] and IL-6 [20–22]. The third term accounts for the activation of macrophages by IFN-γ [23], which is enhanced by TNF-α [31].

Equation for T cells (T)

The density of T cells in $\Omega_M \cup \Omega_A$ satisfies the equation

$$\frac{\partial T}{\partial t} + \nabla \cdot (\mathbf{v}T) - D_T \Delta T = \underbrace{\lambda_T \frac{I_{12}}{1 + I_{10}/K_{I_{10}}} M}_{activtion} \underbrace{-d_T T}_{death}. \tag{3}$$

We assume that T cells are activated by contact with macrophages in IL-12 environment, while IL-12 is inhibited by IL-10 [30].

Equation for SMCs (S)

The equation of the SMCs density in Ω_M is given by

$$\frac{\partial S}{\partial t} + \nabla \cdot (\mathbf{v}S) - D_S \Delta S = \underbrace{\lambda_S - d_{SM} \frac{M}{M + K_M}}_{apoptosis} S - d_S S. \tag{4}$$

The second term of the right-hand side accounts for apoptosis of SMCs, caused by macrophages through a FasL/Fas-Caspase8-RIP1 mediated mechanism [19].

Equations for cytokines (in $\Omega_M \cup \Omega_A$)

IL-6 is produced by macrophages [26], and by SMCs (in conjunction with IL-1) [18]; hence

$$\frac{\partial I_6}{\partial t} - D_{I_6} \Delta I_6 = \underbrace{\lambda_{I_6 M} M + \lambda_{I_6 S} S}_{production} \underbrace{-d_{I_6} I_6}_{degradation}. \tag{5}$$

IL-10 is produced by macrophages [26], so that

$$\frac{\partial I_{10}}{\partial t} - D_{I_{10}}\nabla^2 I_{10} = \underbrace{\lambda_{I_{10}M} M}_{production} \underbrace{-d_{I_{10}} I_{10}}_{degradation}. \quad (6)$$

IL-12 is produced by macrophages [26], a process inhibited by IL-10. The equation for I_{12} is given by

$$\frac{\partial I_{12}}{\partial t} - D_{I_{12}}\nabla^2 I_{12} = \underbrace{\lambda_{I_{12}M}\frac{M}{1+I_{10}/K_{I_{10}}}}_{\text{production by macrophage}} \underbrace{-d_{I_{12}} I_{12}}_{degradation}. \quad (7)$$

Similarly, TNF-α is produced by macrophages, a process inhibited by IL-10 [32], so that

$$\frac{\partial T_\alpha}{\partial t} - D_{T_\beta}\Delta T_\alpha = \underbrace{\lambda_{T_\alpha M}\frac{M}{1+I_{10}/K_{I_{10}}}}_{production} \underbrace{-d_{T_\alpha} T_\alpha}_{degradation}. \quad (8)$$

IFN-γ is produced by T cells [33], hence

$$\frac{\partial I_\gamma}{\partial t} - D_{I_\gamma}\Delta I_\gamma = \underbrace{\lambda_{I_\gamma} T}_{production} \underbrace{-d_{I_\gamma} I_\gamma}_{degradation}. \quad (9)$$

MMP is produced by macrophages [25] and by SMCs [34], a process enhanced by TNF-α [24], and MMP is lost by binding with TIMP [25]. Accordingly, Q satisfies the following equation:

$$\frac{\partial Q}{\partial t} - D_Q\Delta Q = \underbrace{(\lambda_{QM}M + \lambda_{QS}S)\left(1+\lambda_{QT_\alpha}\frac{T_\alpha}{T_\alpha+K_{T_\alpha}}\right)}_{production} \underbrace{-d_{QQ_r}Q_r Q}_{depletion} \underbrace{-d_Q Q}_{degradation}, \quad (10)$$

TIMP is produced by macrophages [25], and is lost by binding to MMP, so that

$$\frac{\partial Q_r}{\partial t} - D_{Q_r}\Delta Q_r = \underbrace{\lambda_{Q_rM}M}_{production} \underbrace{-d_{Q_rQ}QQ_r}_{depletion} \underbrace{-d_{Q_r}Q_r}_{degradation}. \quad (11)$$

Equation for ECM (ρ)

SMCs produce elastin [29] and fibroblasts produce collagen [28]. We assume that the density of fibroblasts is approximately constant, and that the ECM concentration is proportional to the combined concentrations of collagen and elastin, which are produced by fibroblasts and SMCs, respectively. Hence,

$$\frac{\partial \rho}{\partial t} + \nabla\cdot(\mathbf{v}\rho) - D_\rho\Delta\rho = \underbrace{\left[\lambda_{\rho f}\chi_A + \lambda_{\rho S}S\right]\left(1-\frac{\rho}{\rho_0}\right)^+}_{production} \underbrace{-d_\rho\rho - d_{\rho Q}Q\rho}_{degradation}, \quad (12)$$

where the term $d_{\rho Q}\,Q\rho$ represents ECM degradation by MMP. Here we used the notations: $X^+ = X$ if $X > 0$, $X^+ = 0$ if $X \le 0$, and $\chi_A = 1$ in Ω_A, $\chi_A = 0$ in Ω_M.

Boundary conditions

Fig 3 shows a 2-D projection of the media and adventitia layers of the arterial wall. We shall take as our computational domain the right region lying between $y = y_1$ and $y = y_2$, and impose periodic boundary condition at $y = y_1$ and $y = y_2$.

T cells, which are primarily CD4+ Th1 cells [35], migrate to the adventitia and intima [36, 37], and so do macrophages [22, 37].

The concentration ρ is continuous across the media/adventitia membrane, while S satisfies no-flux boundary condition, $\frac{\partial S}{\partial n} = 0$, at this membrane. All the other variables satisfy the following flux conditions at the interface Γ_M:

$$\frac{\partial X_M}{\partial \mathbf{n}} + \gamma(X_M - X_A) = 0, \text{ and } \frac{\partial X_A}{\partial \mathbf{n}} + \gamma(X_A - X_M) = 0,$$

where X_M and X_A are the concentrations of cytokines or cell densities in media and adventitia, respectively. We take $\gamma = 50$ for cells, and $\gamma = 500$ for the cytokines [38].

On Γ_B and Γ_A, we have

$$\frac{\partial M}{\partial \mathbf{n}} + \alpha_M(P)(M - M_0) = 0, \quad \frac{\partial T}{\partial \mathbf{n}} + \alpha_T(T - T_0) = 0,$$

where $\alpha_M(P) = \tilde{\alpha}_M \frac{P}{P+K_P}$.

Both MCP-1 and IL-6 are produced by endothelial cells [17], which lie near the inner boundary of the media, Γ_B. Hence

$$\frac{\partial P}{\partial \mathbf{n}} + \alpha_P(P - P_0) = 0, \quad \frac{\partial I_6}{\partial \mathbf{n}} + \alpha_{I_6}(I_6 - I_{60}) = 0 \text{ on } \Gamma_B, \tag{13}$$

where P_0 and I_{60} are the concentrations of MCP-1 and I_6 in the blood. We assume no-flux boundary conditions on Γ_B for all remaining variables. We also assume no-flux conditions on Γ_A for all variables (except M and T, as stated above)

Initial conditions

We take initially $I_6 = \frac{I_{60}}{2}$, where $I_{60} = 6 \times 10^{-9}\ gcm^{-3}$ in the source of influx of I_6 from the endothelial cells [39], and as in [40],

$$Q = 3 \times 10^{-8},\ Q_r = 10^{-8},\ \rho = 3.43 \times 10^{-4} \text{ and } S = S_0,\ \text{where } S_0 = 6 \times 10^{-3}\ gcm^{-3}.$$

All other cell densities and cytokine concentrations are taken to be zero initially. We prescribe the initial geometry of aneurysm by

$$\Gamma_A:\ x = 0.7\cos(\pi y)^2 + 0.3,\ \Gamma_M:\ x = 0.55\cos(\pi y)^2 + 0.2,$$
$$\Gamma_B:\ x = 0.5\cos(\pi y)^2 \text{ for } y_1 \le y \le y_2.$$

Mechanical hyperelasticity model

We set $\Omega = \Omega_M \cup \Gamma_M \cup \Omega_A$ and refer to this region, briefly, as the aortic wall. Aortic wall is assumed to have nonlinear, hyperelastic material properties [27, 41, 42]. Specifically, it is an 'almost' incompressible, homogeneous, and isotropic material with energy density function W of the form

$$W = \beta_1(\mathbf{I_B} - 3) + \beta_2(\mathbf{I_B} - 3)^2, \tag{14}$$

where β_1 and β_2 are forces that represent elastic coefficients; $\mathbf{I_B}$ is the first invariant of the Left Cauchy-Green tensor $\mathbf{B}$ (namely $\mathbf{I_B} = tr(\mathbf{B})$), $\mathbf{B} = \mathbf{F}\,\mathbf{F}^T$, while $\mathbf{F}$ is the deformation gradient tensor. In terms of the displacement vector $\mathbf{u} = (u_i)$, we can write $B = [(I - \nabla\mathbf{u})^T(I - \nabla\mathbf{u})]^{-1} = \left(\delta_{ij} - \frac{\partial u_j}{\partial x_i} - \frac{\partial u_i}{\partial x_j} + \frac{\partial u_k}{\partial x_i}\frac{\partial u_k}{\partial x_j}\right)^{-1} \doteq (a_{ij})^{-1}$, where $\mathbf{I}$ is the identity tensor.

The Cauchy stress tensor is given by

$$\sigma = -pI + 2\frac{\partial W}{\partial \mathbf{I_B}}\mathbf{B}, \tag{15}$$

where p is the hydrostatic pressure. The momentum equation is then

$$dD_t\mathbf{v} - \nabla\cdot\sigma \quad = \mathbf{f} \quad \text{in } \Omega, \tag{16}$$

where $\mathbf{f}$ is the body force and d is the tissue density. In the sequel we assume no body force and neglect tissue inertia, so that

$$\nabla\cdot\sigma \quad = 0, \quad \text{in } \Omega. \tag{17}$$

The coefficients β_1 and β_2 are functions of the SMCs which we take to represent the elasticity coefficients. We shall use the following specific relations in Eq (14):

$$\beta_1 = \beta_{10} + k_1\left(\frac{S}{S_0} - 1\right), \quad \beta_2 = \beta_{20} + k_2\left(\frac{S}{S_0} - 1\right). \tag{18}$$

The pressure, p, is a function of ECM, which we take to have the form

$$p(\rho) = p^* - \beta_p\left(1 - \frac{\rho}{\rho^*}\right). \tag{19}$$

for some parameters β_p, p^*.

For boundary conditions, we take

$$\begin{aligned} \sigma\mathbf{n} &= \sigma_B\mathbf{n} - \gamma\kappa\mathbf{n} \text{ on } \Gamma_B, \\ (\sigma\mathbf{n})|_{\Omega_M} &= (\sigma\mathbf{n})|_{\Omega_A} + \gamma\kappa\mathbf{n} \text{ on } \Gamma_M, \end{aligned} \tag{20}$$

$$\sigma\mathbf{n} = 0 \text{ on } \Gamma_A, \tag{21}$$

where σ_B is the stress tensor from the blood and κ is the mean curvature.

Results

Fig 4 shows the profile of average of cell densities and cytokines concentrations in the first 500 days, and Fig 5 shows how the aneurysm deforms at day 500.

From Fig 4, we see that, as AAA progresses, the average densities of SMCs and ECM decrease. The concentration of the inflammatory cytokines TNF-α, IFN-γ and MCP-1 are increasing. On the other hand, the average concentration of MMP is increasing only for the first 200 days, and it then decreases as the concentration of TIMP keeps growing. The average concentration of IL-6 in the tissue decreases and nearly stabilizes after 500 days. Fig 5 shows growth of the aorta bulge after 500 days: from diameter of 2 cm to diameter of nearly 2.5 cm when $I_{60} = 6 \times 10^{-9}$ g/ml and nearly 4.5 cm when $I_{60} = 6 \times 10^{-8}$ g/ml.

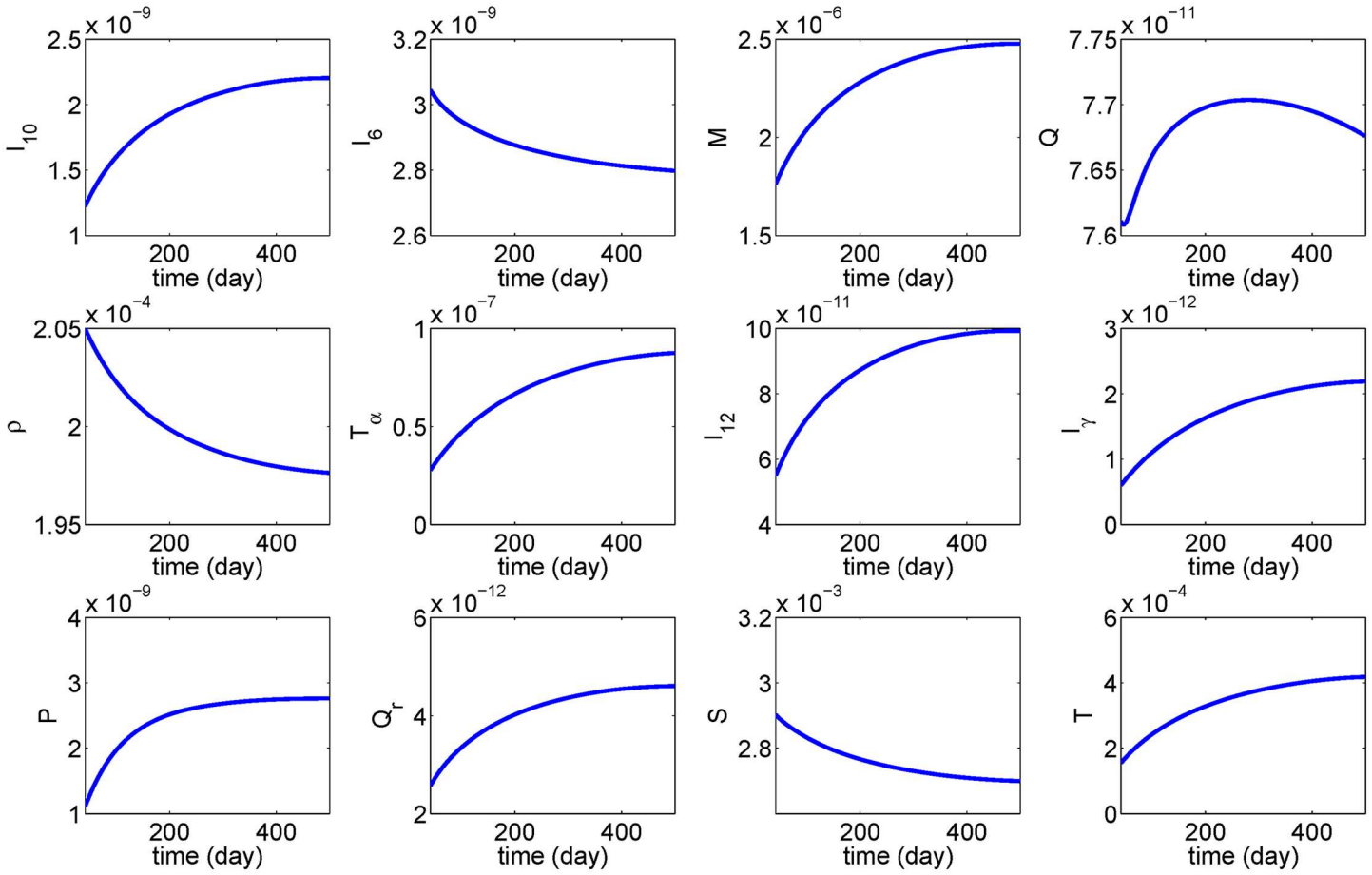

Fig 4. Simulation results over 500 days. The parameter used are as in Tables 2 and 3 with $I_{60} = 6 \times 10^{-9}$ g/ml.

doi:10.1371/journal.pone.0170807.g004

In Figs 4 and 5, the initial values of the pro-inflammatory cytokines were taken to be below their steady state. On the other hand the SMCs and ECM densities were taken to be above their steady state. Other choices of the initial conditions yield similar profiles (not shown here).

If at the initial screening for AAA we measure both the aorta diameter, R_0, and the concentration of IL-6 in the blood, I_{60}, then by simulating the model with these values of $R(0) = R_0$ and I_{60} (in Eq (13)), we can predict the AAA diameter at any future time T. Figs 6 and 7 simulate the cases $T = 300$ and $T = 500$ days. Thus, for every pair of I_{60} (on the horizontal axis) and R_0 (on the vertical axis) the color on the column shows the diameter corresponding to the point (I_{60}, R_0) at day $T = 300$ (upper) and $T = 500$ (lower).

Conclusions

Abdominal aortic aneurysm is a localized enlargement of the abdominal aorta, which may lead to rupture of the aorta. The disease is asymptomatic until rupture, which is nearly always fatal. The risk of rupture associated with the increased diameter of the aorta varies among people. Hence it is difficult to determine, on the basis of just the current diameter (R_0) of a patient's

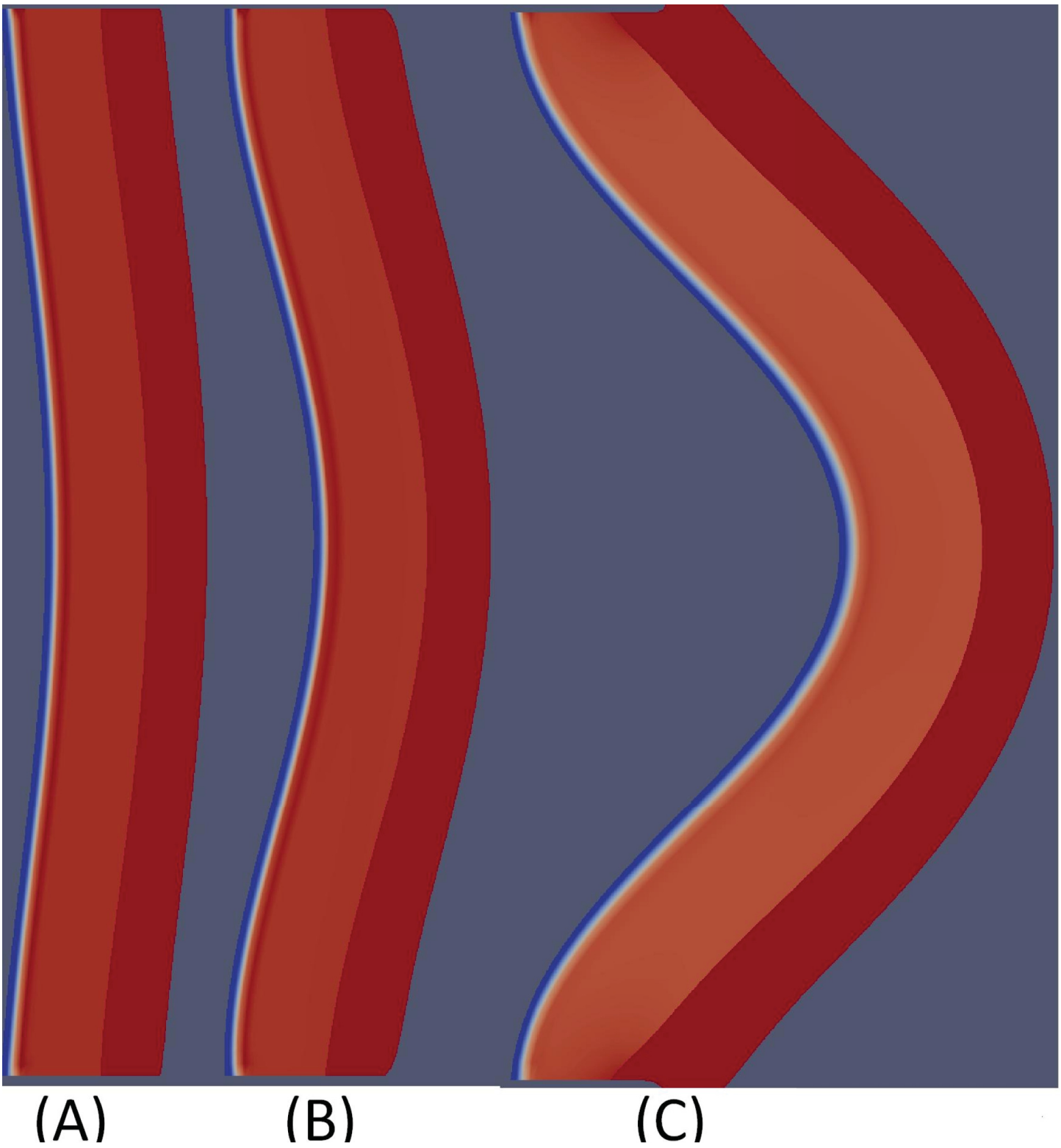

Fig 5. Aneurysm deformation at day 500 with initial deformation shown in (A). The parameters used are as in Tables 2 and 3 with (B) $I_{60} = 6 \times 10^{-9}$ g/ml, and (C) $I_{60} = 6 \times 10^{-8}$ g/ml. The diameter grows from 2 cm to 2.5 cm in case (B), and to 4.5 cm in case (C).

doi:10.1371/journal.pone.0170807.g005

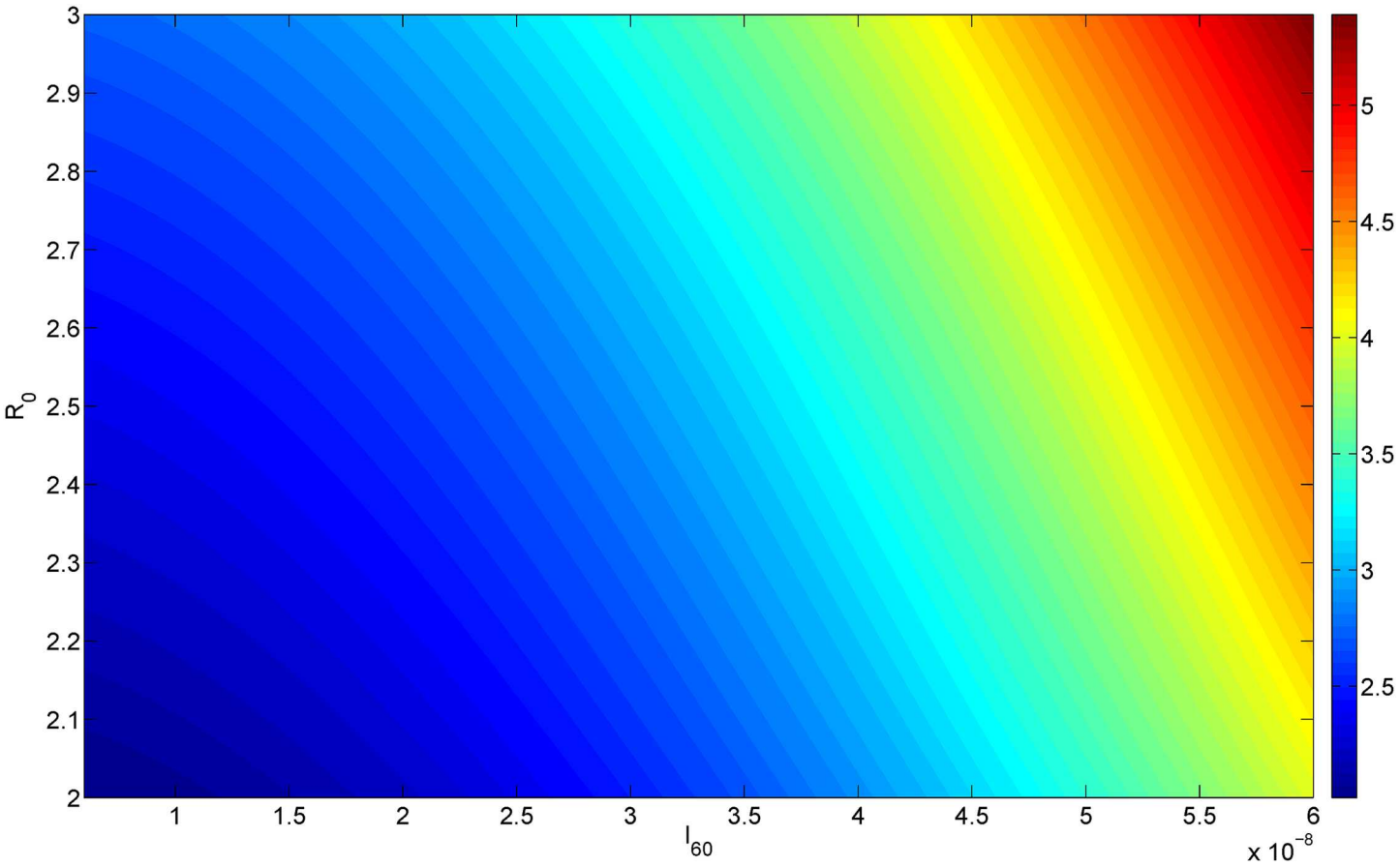

Fig 6. AAA growth. The x-axis scales I_{60} from 6×10^{-9} g/ml to 6×10^{-8} g/ml; the y-axis scales R_0 from 2 cm to 3 cm; The color represents the diameter of aortic bulge at 300 day.

doi:10.1371/journal.pone.0170807.g006

aortic wall, how closely this patient's abdominal aorta should be monitored. In order to make such a determination, we need address the following questions:

- how fast the diameter will grow over time?
- how does the risk of rupture depend on the growing diameter?

Several non-invasive prognostic biomarkers for AAA have been suggested [13, 14]; specifically, IL-6 [11, 12].

The present paper addresses the first question with a mathematical model: Given R_0 and the serum concentration of IL-6, the model predicts the dynamical growth of the diameter, $R(t)$, for any future time t. The mathematical model includes the basic biology underlying AAA formation as a disease that degrades the elastic strength of the aortic wall. Simulations of the model can show how the initial diameter R_0 and the serum concentration of IL-6 determine the diameter R after a given period of time T; This is done in Fig 6 in the cases of $T = 300$ days and $T = 500$ days. Thus, the level of IL-6 concentration in the blood can be used to suggest how soon to schedule the next screening of the patient's abdominal aorta.

The model is represented by a system of partial differential equations, based on some simplified assumptions. In particular, the model assumes that the disease is associated with initial inflammation, and that the aortic wall is a 'pure' hyperelastic material. Furthermore, some of

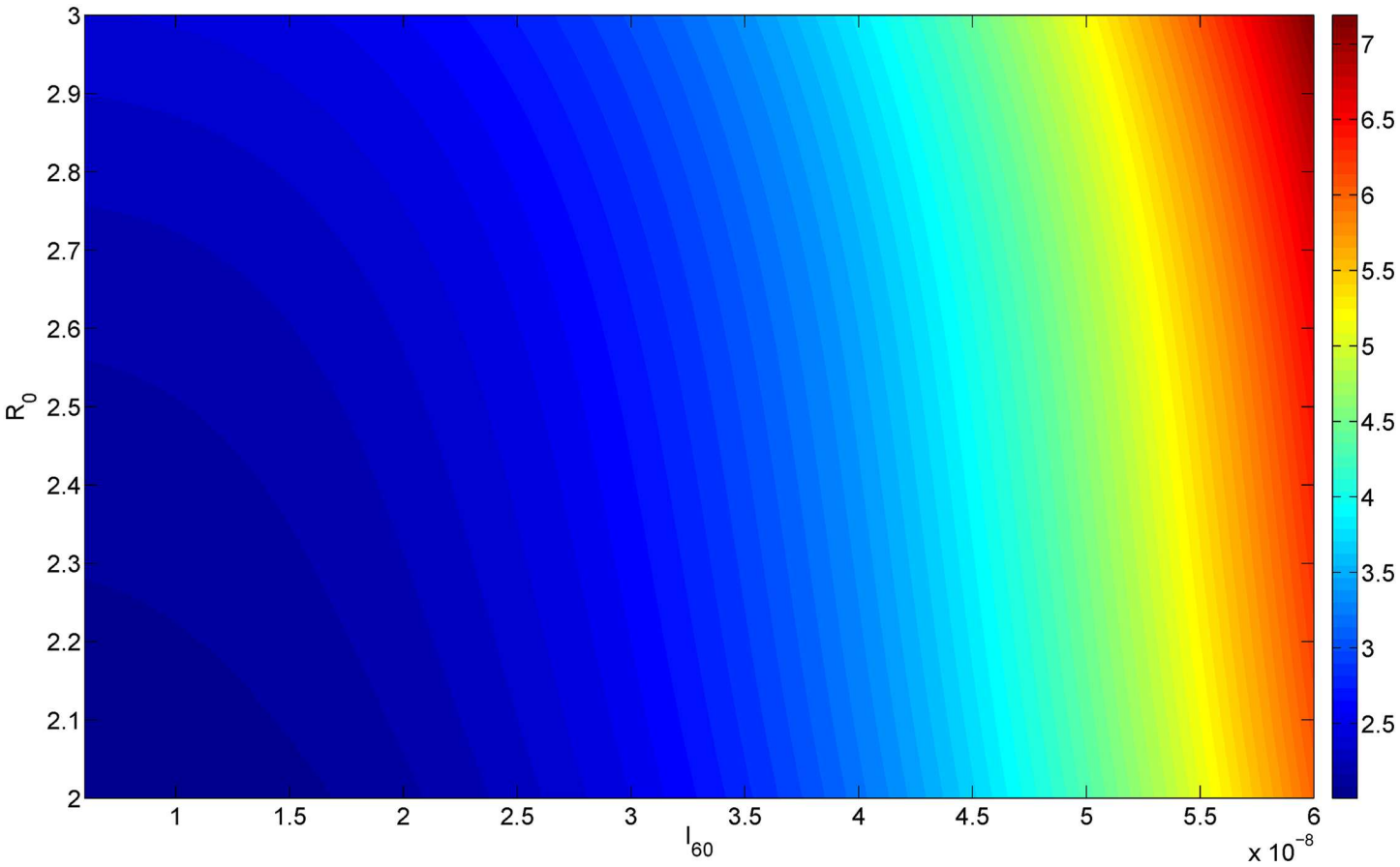

Fig 7. AAA growth. The x-axis scales I_{60} from 6 × 10^{-9} g/ml to 6 × 10^{-8} g/ml; the y-axis scales R_0 from 2 cm to 3 cm; The color represents the diameter of aortic bulge at 500 day.

doi:10.1371/journal.pone.0170807.g007

the parameters were estimated crudely, for the lack of available data. The authors plan to follow up this study with patients data, which are unavailable at this time. The patients will be followed every 6 months with CT scan and measurement of their aneurysm, and of course any patient who comes for surgery or rupture will be recorded. When patients data become available, the model could then be refined, in particular by adjusting some parameters for specific groups of patients. The model could then be used as a predictive tool for monitoring the enlargement of the abdominal aorta.

Parameter estimates

All the parameter values are listed in Tables 2 and 3. Most parameters are taken from the literature while some are estimated below. A few remaining parameters are fitted.

$\lambda_{I_6 M}$ and $\lambda_{I_6 S}$

According to [16], 10^6 macrophages produced 10 ng/ml of IL-6. Assuming steady state, we have

$$\lambda_{I_6 M} M - d_{I_6} I_6 = 0.$$

Table 2. Parameters' description and value.

Parameter	Description	Value
D_M	dispersion coefficient of macrophages	8.64×10^{-7} cm^2 day^{-1} [40, 46, 47]
D_T	diffusion coefficient of T-cell	8.64×10^{-7} cm^2 day^{-1} [40, 46, 47]
D_{I_γ}	diffusion coefficient of IFN-γ	1.08×10^{-2} cm^2 day^{-1} [40, 46, 47]
D_{T_α}	diffusion coefficient for TNF-α	1.29×10^{-2} cm^2 day^{-1} [47]
D_S	diffusion coefficient of SMCs	8.64×10^{-7} cm^2 day^{-1} [40, 46]
D_P	diffusion coefficient of MCP-1	1.728×10^{-1} cm^2 day^{-1} [40, 46]
D_Q	diffusion coefficient of MMP	4.32×10^{-2} cm^2 day^{-1} [40, 46]
D_{Q_r}	diffusion coefficient for TIMP	4.32×10^{-2} cm^2 day^{-1} [40, 46]
D_{I_6}	diffusion coefficient of IL-10	1.08×10^{-2} cm^2 day^{-1} [40, 46, 47]
$D_{I_{10}}$	diffusion coefficient of IL-10	1.08×10^{-2} cm^2 day^{-1} [40, 46, 47]
$D_{I_{12}}$	diffusion coefficient of IL-12	1.08×10^{-2} cm^2 day^{-1} [40, 46, 47]
$\lambda_{T_\alpha M}$	activation rate of TNF-α duetomacrophage	2.86×10^{-3} day^{-1} [47]
λ_{MI_γ}	activation rate of macrophages by IFN-γ	0.005 day^{-1} [40, 46]
λ_T	activation rate of Th1 cells by IL-12	6×10^{-4} day^{-1} [47]
$\lambda_{I_6 M}$	production rate of IL-6 by macrophages	1.73×10^{-6} day^{-1} [16] & estimated
$\lambda_{I_6 S}$	production rate of IL-6 by SMCs	1.73×10^{-5} day^{-1} [18] & estimated
$\lambda_{I_\gamma T}$	production rate of IFN-γ by T cells	2.34×10^{-6} day^{-1} [47]
$\lambda_{I_{12} M}$	production rate of IL-12 by macrophages	3.78×10^{-3} day^{-1} [47]
$\lambda_{I_{10} M}$	production rate of IL-10 by macrophages	2×10^{-3} day^{-1} [47]
λ_{QM}	production rate of MMP by macrophages	3×10^{-4} day^{-1} [48]
λ_{QS}	production rate of MMP by SMCs	2.16×10^{-5} day^{-1} [40, 46]
λ_{QT_α}	production rate of MMP by TNF-α	2 fitted
$\lambda_{Q_r M}$	production rate of TIMP by macrophages	6×10^{-5} day^{-1} [40, 46]
λ_{PS}	activation rate of MCP-1 due to SMCs	3×10^{-3} day^{-1} fitted
$\lambda_{\rho f}$	activation rate of ECM due to fibroblasts	3×10^{-4} day^{-1} [40]
$\lambda_{\rho S}$	activation rate of ECM due to SMCs	1×10^{-1} day^{-1} fitted
d_M	death rate of macrophages	0.015 day^{-1} [40, 46, 47]
d_ρ	degradation rate of ECM	0.37 day^{-1} [40, 46, 47]
d_P	degradation rate of MCP-1	1.73 day^{-1} [40, 46, 47]
d_{PM}	internalization rate of MCP-1 by macrophages	2.08×10^{-4} day^{-1} [40, 46, 47]
d_{QQ_r}	binding rate of MMP to TIMP	4.98×10^{8} cm^3 g^{-1} day^{-1} [40, 46, 47]
$d_{Q_r Q}$	binding rate of TIMP to MMP	1.04×10^{9} cm^3 g^{-1} day^{-1} [40, 46, 47]
d_Q	degradation rate of MMP	4.32 day^{-1} [40, 46, 47]
d_{Q_r}	degradation rate of TIMP	21.6 day^{-1} [40, 46, 47]
$d_{\rho Q}$	degradation rate of ECM due to MMP	2.59×10^{7} cm^3 g^{-1} day^{-1} [40, 46, 47]
d_{I_γ}	degradation rate of IFN-γ	0.69 day^{-1} [46]
d_S	death rate of SMC	0.86 day^{-1} [40, 46, 47]
d_{SM}	apoptosis rate of SMC by macrophages	1.72 day^{-1} fitted
$d_{I_{12}}$	degradation rate of IL-12	1.188 day^{-1} [40, 46, 47]
d_{T_α}	degradation rate of TNF-α	55.45 day^{-1} [40, 46, 47]
d_{I_6}	degradation rate of IL-6	0.173 day^{-1} [43]
$d_{I_{10}}$	degradation rate of IL-10	16.64 day^{-1} [47]

doi:10.1371/journal.pone.0170807.t002

Table 3. Parameters' description and value.

Parameter	Description	Value
χ_C	chemotactic sensitivity parameter by MCP-1	10 $cm^5\ g^{-1}$ day^{-1} [40, 46, 47]
K_M	macrophage saturation	5×10^{-5} gcm^{-3} [40]
K_P	MCP-1 saturation for influx of macrophages	5×10^{-9} gcm^{-3} [40]
K_{I_γ}	IFN-γ saturation for activation of macrophages	1×10^{-11} gcm^{-3} [40]
$K_{I_{10}}$	IL-10 saturation	2×10^{-7} g/cm^3 [47]
K_{T_α}	TNF-α saturation	5×10^{-7} g/cm^3 [47]
ρ_0	ECM saturation	10^{-3} gcm^{-3} [40]
M_0	source/influx of macrophages from blood	5×10^{-5} gcm^{-3} [40]
T_0	source/influx of T cells into intima	1×10^{-3} gcm^{-3} [40]
P_0	MCP-1 concentration	3×10^{-10} [40]
$\tilde{\alpha}$	influx rate of macrophages into interstitium	0.2 cm^{-1} [40]
α_T	influx rate of T cell into interstitium	0.2 cm^{-1} [40]
α_{I_6}	influx rate of IL-6 into interstitium	0.2 cm^{-1} [40]
α_P	influx rate of MCP-1 into interstitium	0.2 cm^{-1} [40]
γ	influx rate of media into adventitia	0.1 cm^{-1} [40]
S_0	initial steady state of SMCs	6×10^{-3} gcm^{-3} [40]
I_{60}	source/influx of IL-6	$6 \times 10^{-9} \sim 6 \times 10^{-8}$ gcm^{-3} [39]
β_{10}	Coefficient of AAA tissue material properties	17.4 N/cm^2 [42] and estimated
β_{20}	Coefficient of AAA tissue material properties	188.1 N/cm^2 [42] and estimated
k_1	Coefficient of AAA tissue material properties	30.4 N/cm^2 [42] and estimated
k_2	Coefficient of AAA tissue material properties	84 N/cm^2 [42] and estimated
β_p	pressure parameter	18.0 N/cm^2 [44] and estimated

doi:10.1371/journal.pone.0170807.t003

Since $d_{I_6} = 0.173$ day^{-1} [43], we get $\lambda_{I_6 M} = 1.73 \times 10^{-6}$ day^{-1}.

According to [18], 4×10^4 cells/ml SMCs produced 4 ng/ml of IL-6. Assuming steady state, we have

$$\lambda_{I_6 S} S - d_{I_6} I_6 = 0.$$

Since $d_{I_6} = 0.173$ day^{-1}, we get $\lambda_{I_6 S} = 1.73 \times 10^{-5}$ day^{-1}.

β_{10}, β_{20}, k_1 and k_2

By [42], $\beta_1 = 0.022\ N/mm^2$ and $\beta_{10} = 0.174\ N/mm^2$. We assume that in aneurysm S is approximately half its normal density, i.e., $S \approx \frac{S_0}{2}$. Then by Eq (17),

$$\beta_1 = \beta_{10} - k_1 \frac{1}{2},$$

which gives $k_1 = 30.4\ N/cm^2$.

Similarly, by [42], $\beta_2 = 1.461\ N/mm^2$ and $\beta_{20} = 1.881\ N/mm^2$ so that

$$\beta_{20} - k_2 \frac{1}{2} = \beta_2 = 1.461\ N/mm^2;$$

hence $k_2 = 84\ N/cm^2$.

β_p

By [44], the peak wall stress measured for normal people and AAA patients were 30-44 N/cm^2 and 28-37 N/cm^2, respectively. We assume that ECM in AAA patients is reduced to 75% of its value in healthy individuals. Hence

$$p^* = \frac{30+44}{2} = 37\ N/cm^2, \text{ and } p\left(\frac{3\rho^*}{4}\right) = \frac{28+37}{2},$$

which implies, by Eq (18), that $\beta_p = 18\ N/cm^2$.

1.1 σ_B

We assume $\sigma_B = -p_B\, I$, where p_B is average central aortic systolic pressure (100-120 mm Hg) [45]; we take $p_B = 110$ mm Hg.

Numerical methods

Weak formulation

In this subsection, we rewrite in compact form the coupled biological and mechanical systems. We denote by Z the vector of the densities or concentrations of cells and cytokines, i.e. $Z = (P, M, T, S, I_6, I_{10}, I_{12}, T_\alpha, I_\gamma, Q, Q_r, \rho)^T$. The entries of Z satisfy advection-diffusion equations with nonlinear source term, as seen from Eqs (1)–(12):

$$D_t Z + (\nabla \cdot \mathbf{v})Z - \nabla \cdot (D_Z \nabla Z) = F(Z), \qquad \text{in } \Omega_M(t) \cup \Omega_A(t), \tag{22}$$

where the velocity $\mathbf{v}$ is defined by $\mathbf{v} = D_t\, \mathbf{u}$, where D_t denotes the material derivative,

$$D_t = \partial_t + \mathbf{v} \cdot \nabla.$$

In the equation for Z, $F(Z)$ is a source term and D_Z is a diagonal matrix with the diagonal terms for the diffusion coefficients of the biological species.

Some of the components of Z live only in either $\Omega_M(t)$ or $\Omega_A(t)$. Since there is a jump for Z at the media/adventitia interface, $\Gamma_M(t)$, we split Z into two parts

$$Z_M = Z|_{\Omega_M(t)} \quad \text{and} \quad Z_A = Z|_{\Omega_A(t)}.$$

The boundary conditions can then be written in the form

$$\begin{cases} \dfrac{\partial Z_A}{\partial \mathbf{n}} = 0, & \text{on } \Gamma_A(t), \\ \dfrac{\partial Z_M}{\partial \mathbf{n}} = \tilde{\gamma}(Z_0 - Z_M), & \text{on } \Gamma_B(t), \\ \dfrac{\partial Z_M}{\partial \mathbf{n}} = \tilde{\gamma}(Z_A - Z_M), & \text{on } \Gamma_M(t), \\ \dfrac{\partial Z_A}{\partial \mathbf{n}} = \tilde{\gamma}(Z_M - Z_A), & \text{on } \Gamma_M(t) \end{cases}$$

for an appropriate coefficient $\tilde{\gamma}$, some of its component being zero.

The governing equation for the displacement $\mathbf{u}$ can be written as

$$\nabla \cdot \sigma(\mathbf{u}) \quad = 0, \qquad \text{in } \Omega_M(t) \cup \Omega_A(t), \tag{23}$$

where the stress σ is is defined in terms of the displacement by

$$\sigma(\mathbf{u}) = -p(\rho)\mathbf{I} + (2\beta_1(S) + 4\beta_2(S)(\mathrm{tr}(\mathbf{B}) - 3))\mathbf{B}.$$

with the boundary conditions

$$\begin{cases} \mathbf{u} &= 0, & \text{on } \Gamma_0, \\ \mathbf{u}_M &= \mathbf{u}_A, & \text{on } \Gamma_M(t), \\ \sigma\mathbf{n} &= 0, & \text{on } \Gamma_0 \cup \Gamma_A(t), \\ \sigma\mathbf{n} &= \sigma_B\mathbf{n} - \gamma\kappa\mathbf{n}, & \text{on } \Gamma_B(t), \\ (\sigma\mathbf{n})|_{\Omega_M} &= (\sigma\mathbf{n})|_{\Omega_A} + \gamma\kappa\mathbf{n} & \text{on } \Gamma_M(t). \end{cases}$$

Multiplying the coupled System (22) and (23) by arbitrary test functions (W_M, W_A,$\mathbf{w}$), and performing integration by parts using the boundary conditions, we get the weak formulation:

$$\begin{cases} (D_t Z_M, W_M)_{\Omega_M(t)} + ((\nabla\cdot\mathbf{v})Z_M, W_M)_{\Omega_M(t)} + (D_Z\nabla Z_M, \nabla W_M)_{\Omega_M(t)} \\ -\langle\gamma(Z_A - Z_M), W_M\rangle_{\Gamma_M(t)} - \langle\alpha_Z(Z_0 - Z_M), W_M\rangle_{\Gamma_B(t)} = (F, W_M)_{\Omega_M(t)}, \\ (D_t Z_A, W_A)_{\Omega_A(t)} + ((\nabla\cdot\mathbf{v})Z_A, W_A)_{\Omega_A(t)} + (D_Z\nabla Z_A, \nabla W_A)_{\Omega_A(t)} \\ -\langle\gamma(Z_M - Z_A), W_A\rangle_{\Gamma_M(t)} = (F, W_A)_{\Omega_A(t)}, \\ (\sigma, \nabla\mathbf{w})_{\Omega(t)} - \langle\sigma_B\mathbf{n} - \gamma\kappa\mathbf{n}, \mathbf{w}\rangle_{\Gamma_B(t)} + \langle\gamma\kappa\mathbf{n}, \mathbf{w}\rangle_{\Gamma_M(t)} = 0. \end{cases} \quad (24)$$

Here we used $(\cdot,\cdot)_D$ and $\langle\cdot,\cdot\rangle_{\partial D}$ to denote the L^2 inner product on the domain D and on the boundary ∂D, respectively.

Lagrangian description for hyperelastic equation

$\Omega_A(t)$, $\Omega_M(t)$ and their boundaries are moving in time. We set $\Omega(t) = \Omega_M(t) \cup \Omega_A(t) \cup \Gamma_M(t)$ and $\hat{\Omega}_M = \Omega_M(0)$, $\hat{\Omega}_A = \Omega_A(0)$, $\hat{\Omega} = \Omega(0)$. To characterize the motion of the media and adventitia, we introduce a flow map $x(\hat{x}, t)$ for the position of the particle $\hat{x}$ at time t.

Then each function can be described in Lagrangian coordinates, namely for each function $f(x, t)$, its Lagrangian description is

$$\hat{f}(\hat{x}, t) = f(x(\hat{x}, t), t).$$

We also introduce the following variables in Lagrangian coordinates: The displacement $\hat{\mathbf{u}}(\hat{x}, t) = \mathbf{u}(x(\hat{x}, t), t) = x(\hat{x}, t) - \hat{x}$, the deformation tensor $F(\hat{x}, t) = \frac{\partial x}{\partial \hat{x}}(\hat{x}, t) = \mathbf{I} + \frac{\partial \hat{\mathbf{u}}}{\partial \hat{x}}(\hat{x}, t)$, and its determinant $J(\hat{x}, t) = \det(F(\hat{x}, t))$.

By change of variables, we can write the weak form for the equilibrium equation for $\mathbf{w}$ in Lagrangian coordinates,

$$(J\hat{\sigma}F^{-T}, \hat{\nabla}\hat{\mathbf{w}})\hat{\Omega} - \langle J\hat{\sigma}_B F^{-T}\hat{\mathbf{n}}, \hat{\mathbf{w}}\rangle_{\Gamma_B(0)} = \langle\gamma\kappa\mathbf{n}, \mathbf{w}\rangle_{\Gamma_M(t)\cup\Gamma_B(t)} \quad (25)$$

where

$$\hat{\sigma} = -J\hat{p}F^{-T} + J(\beta_1(\hat{S}) + 2\beta_2(\hat{S})(\mathrm{tr}(B) - 3))F.$$

As for the surface tension term, we can also write it in the Lagrangian coordinates as follows:

$$\langle \gamma\kappa\mathbf{n}, \mathbf{w}\rangle_{\Gamma(t)} = \int_{\hat{\Gamma}} \gamma J|F^{-T}\hat{\mathbf{n}}|\left(\mathrm{tr}(\hat{\nabla}\mathbf{w}F^{-1}) - \frac{\hat{\mathbf{n}}^T F^{-1}\hat{\nabla}\mathbf{w}F^{-1}F^{-T}\hat{\mathbf{n}}}{|F^{-T}\hat{\mathbf{n}}|^2}\right) d\hat{S}. \tag{26}$$

By substituting this expression into the hyperelasitcity equation in Lagrangian coordinates Eq (25), we can get a nonlinear equation:

$$a_L(\hat{\mathbf{u}}, \hat{\mathbf{w}}; \hat{S}, \hat{\rho}) = 0 \tag{27}$$

Finite element discretization on the moving mesh

In order to deal with the free boundary and the jump at the interface, we use the moving mesh method.

The initial domains $\hat{\Omega}_M$ and $\hat{\Omega}_A$ are discretized by triangulations, denoted by $T^0_{M,h}$ and $T^0_{A,h}$, respectively. We consider the case that $T^0_{M,h}$ and $T^0_{A,h}$ are matching on the interface Γ^0_M. We use piecewise linear and continuous function $\hat{\mathbf{u}}_h$ to approximate the displacement. Then the triangulation $T^n_{M,h} \cup T^n_{A,h}$ for the current domain Ω^n_h can be obtained by moving the grid nodes of $T^0_{M,h} \cup T^0_{A,h}$ according to the flow map $x(\hat{x}, t) = \hat{x} + \hat{\mathbf{u}}_h(\hat{x}, t)$.

We next introduce the following time discretization for the material derivative

$$(\widehat{D_t Z})^n \approx (\widehat{D_{t,k} Z})^n := \frac{Z(x(\hat{x}, t^n), t^n) - Z(x(\hat{x}, t^{n-1}), t^{n-1})}{k},$$

and for

$$\hat{\mathbf{v}}^n = \widehat{D_t \mathbf{u}}^n \approx \frac{\hat{u}(\hat{x}, t^n) - \hat{u}(\hat{x}, t^{n-1})}{k}$$

where we use the superscript n to indicate the function at time nk, where k is the time step. Note that no interpolation is needed for evaluating the material derivative $D_{t,k}$ at grid points, since the grid points are moving according to the flow map.

For the space discretization, we use piecewise linear and continuous function spaces $\mathcal{V}_h$, $\mathcal{W}^n_{h,M}$ and $\mathcal{W}^n_{h,A}$ to approximate the solutions. Let $\{\hat{\mathbf{w}}_i\}_{i=1}^N$, $\{W^n_{M,i}\}_{i=1}^{N_M}$ and $\{W^n_{A,i}\}_{i=1}^{N_A}$ be the bases of $\mathcal{V}_h$, $\mathcal{W}^n_{h,M}$ and $\mathcal{W}^n_{h,A}$, respectively, where N, N_M and N_A are the numbers of basis functions of the corresponding spaces. The approximation solutions at time nk can be written as summations

$$Z^n_{M,h} = \sum_{i=1}^{N_M} c^n_{M,i} W^n_{M,i},$$

$$Z^n_{A,h} = \sum_{i=1}^{N_A} c^n_{A,i} W^n_{A,i},$$

$$\hat{\mathbf{u}}^n_h = \sum_{i=1}^{N} c^n_i \hat{\mathbf{w}}^n_i,$$

with coefficients to be determined by the discrete system, corresponding to the System (24),

$$\begin{cases} ((D_{t,k}Z_M)_h^n, W_M)_{\Omega_M^n} + ((\nabla \cdot \mathbf{v}_h^n)Z_{M,h}^n, W_M)_{\Omega_M^n} + (D_Z \nabla Z_{M,h}^n, \nabla W_M)_{\Omega_M^n} \\ -\langle \gamma(Z_{A,h}^n - Z_{M,h}^n), W_M \rangle_{\Gamma_M^n} - \langle \alpha_Z(Z_0 - Z_{M,h}^n), W_M \rangle_{\Gamma_B^n} = (F_h^{n-1}, W_M)_{\Omega_M^n}, \\ ((D_{t,k}Z_A)_h^n, W_A)_{\Omega_A^n} + ((\nabla \cdot \mathbf{v}_h^n)Z_{A,h}^n, W_A)_{\Omega_A^n} + (D_Z \nabla Z_{A,h}^n, \nabla W_A)_{\Omega_A^n} \\ -\langle \gamma(Z_{M,h}^n - Z_{A,h}^n), W_A \rangle_{\Gamma_M^n} = (F_h^{n-1}, W_A)_{\Omega_A^n}, \\ a_L(\hat{\mathbf{u}}_h^n, \hat{\mathbf{w}}; \hat{S}_h^{n-1}, \hat{\rho}_h^{n-1}) = 0, \end{cases} \tag{28}$$

for any $\hat{\mathbf{w}} \in \mathcal{V}_h$, $W_M \in \mathcal{W}_{h,M}^n$ and $W_A \in \mathcal{W}_{h,A}^n$. Here we use the explicit discretization of the coefficients for the elasticity, and the source terms for the biological species. We denote the first two equations in Eulerian coordinates of the System (28) by

$$a_E(Z_h^n, W; Z_h^{h-1}, \mathbf{v}_h^n, F_h^{n-1}, \Omega_h^n) = 0.$$

By this discretization, the elastic equation and the biological equation are decoupled. Given the solutions in last time step, we use the Newton's nonlinear iteration method to solve the system $a_L = 0$ in the initial domain. Then we update the triangulations for the current domain Ω_h^n by the approximate flow map $x(\hat{x}, t) = \hat{x} + \hat{\mathbf{u}}_h(\hat{x}, t)$. Following the standard technique of finite element method, we then solve the variational problem $a_E = 0$ for the biological species. We thus get the solution of current time step.

Author Contributions

Conceptualization: WH AF MG JX.

Funding acquisition: DZ.

Investigation: WH AF MG.

Methodology: SW SG JX.

Project administration: WH JX.

Resources: MG.

Software: DZ.

Validation: WH AF MG.

Visualization: WH SW SG.

Writing – original draft: WH AF SW SG.

Writing – review & editing: WH AF SW SG AF MG JX DZ.

References

1. McGregor JC, Pollock JG, Anton HC. The diagnosis and assessment of abdominal aortic aneurysms by ultrasonography. Ann R Coll Surg Engl. 1976; 58(5):388–392. PMID: 970885
2. Filardo G, Powell JT, Martinez MA, Ballard DJ. Surgery for small asymptomatic abdominal aortic aneurysms. Cochrane Database Syst Rev. 2012; 3:CD001835. doi: 10.1002/14651858.CD001835.pub3 PMID: 22419281

3. Veith FJ, Ohki T, Lipsitz EC, Suggs WD, Cynamon J. Treatment of ruptured abdominal aneurysms with stent grafts: a new gold standard? Semin Vasc Surg. 2003; 16(2):171–175. doi: 10.1016/S0895-7967(03)00003-6 PMID: 12920689
4. No authors listed. Mortality results for randomised controlled trial of early elective surgery or ultrasonographic surveillance for small abdominal aortic aneurysms.. The UK Small Aneurysm Trial Participants Lancet. 1998; 352(9141):1649–1655. doi: 10.1016/S0140-6736(98)10137-X PMID: 9853436
5. Bush RL, Johnson ML, Collins TC, Henderson WG, Khuri SF, Yu HJ, et al. Open versus endovascular abdominal aortic aneurysm repair in VA hospitals. J Am Coll Surg. 2006; 202(4):577–587. doi: 10.1016/j.jamcollsurg.2006.01.005 PMID: 16571424
6. Nicholls SC, Gardner JB, Meissner MH, Johansen HK. Rupture in small abdominal aortic aneurysms. J Vasc Surg. 1998; 28(5):884–888. doi: 10.1016/S0741-5214(98)70065-5 PMID: 9808857
7. Grytsan A, Watton PN, Holzapfel GA. A thick-walled fluid-solid-growth model of abdominal aortic aneurysm evolution: application to a patient-specific geometry. J Biomech Eng. 2015; 137(3). doi: 10.1115/1.4029279 PMID: 25473877
8. Schmid H, Grytsan A, Poshtan E, Watton PN, Itskov M. Influence of differing material properties in media and adventitia on arterial adaptation–application to aneurysm formation and rupture. Comput Methods Biomech Biomed Engin. 2013; 16(1):33–53. doi: 10.1080/10255842.2011.603309 PMID: 22149119
9. Volokh KY. Modeling failure of soft anisotropic materials with application to arteries. J Mech Behav Biomed Mater. 2011; 4(8):1582–1594. doi: 10.1016/j.jmbbm.2011.01.002 PMID: 22098860
10. Watton PN, Hill NA, Heil M. A mathematical model for the growth of the abdominal aortic aneurysm. Biomech Model Mechanobiol. 2004; 3(2):98–113. doi: 10.1007/s10237-004-0052-9 PMID: 15452732
11. Jones KG, Brull DJ, Brown LC, Sian M, Greenhalgh RM, Humphries SE, et al. Interleukin-6 (IL-6) and the prognosis of abdominal aortic aneurysms. Circulation. 2001; 103(18):2260–2265. doi: 10.1161/01.CIR.103.18.2260 PMID: 11342474
12. Takagi H, Watanabe T, Mizuno Y, Kawai N, Umemoto T. Circulating interleukin-6 levels are associated with abdominal aortic aneurysm presence: a meta-analysis and meta-regression of case-control studies. Ann Vasc Surg. 2014; 28(8):1913–1922. doi: 10.1016/j.avsg.2014.06.058 PMID: 25011090
13. Moris D, Mantonakis E, Avgerinos E, Makris M, Bakoyiannis C, Pikoulis E, et al. Novel biomarkers of abdominal aortic aneurysm disease: identifying gaps and dispelling misperceptions. Biomed Res Int. 2014; 2014:925840. doi: 10.1155/2014/925840 PMID: 24967416
14. Golledge J, Tsao PS, Dalman RL, Norman PE. Circulating markers of abdominal aortic aneurysm presence and progression. Circulation. 2008; 118(23):2382–2392. doi: 10.1161/CIRCULATIONAHA.108.802074 PMID: 19047592
15. Abdul-Hussien H, Hanemaaijer R, Kleemann R, Verhaaren BF, van Bockel JH, Lindeman JH. The pathophysiology of abdominal aortic aneurysm growth: corresponding and discordant inflammatory and proteolytic processes in abdominal aortic and popliteal artery aneurysms. J Vasc Surg. 2010; 51(6):1479–1487. doi: 10.1016/j.jvs.2010.01.057 PMID: 20488324
16. Wang Q, Ni H, Lan L, Wei X, Xiang R, Wang Y. Fra-1 protooncogene regulates IL-6 expression in macrophages and promotes the generation of M2d macrophages. Cell Res. 2010; 20(6):701–712. doi: 10.1038/cr.2010.52 PMID: 20386569
17. Volk T, Hensel M, Schuster H, Kox WJ. Secretion of MCP-1 and IL-6 by cytokine stimulated production of reactive oxygen species in endothelial cells. Mol Cell Biochem. 2000; 206(1-2):105–112. doi: 10.1023/A:1007059616914 PMID: 10839200
18. Loppnow H, Bil R, Hirt S, Schonbeck U, Herzberg M, Werdan K, et al. Platelet-derived interleukin-1 induces cytokine production, but not proliferation of human vascular smooth muscle cells. Blood. 1998; 91(1):134–141. PMID: 9414277
19. Wang Q, Ren J, Morgan S, Liu Z, Dou C, Liu B. Monocyte chemoattractant protein-1 (MCP-1) regulates macrophage cytotoxicity in abdominal aortic aneurysm. PLoS ONE. 2014; 9(3):e92053. doi: 10.1371/journal.pone.0092053 PMID: 24632850
20. Koch AE, Kunkel SL, Pearce WH, Shah MR, Parikh D, Evanoff HL, et al. Enhanced production of the chemotactic cytokines interleukin-8 and monocyte chemoattractant protein-1 in human abdominal aortic aneurysms. Am J Pathol. 1993; 142(5):1423–1431. PMID: 8494046
21. Middleton RK, Bown MJ, Lloyd GM, Jones JL, London NJ, Sayers RD. Characterisation of Interleukin-8 and monocyte chemoattractant protein-1 expression within the abdominal aortic aneurysm and their association with mural inflammation. Eur J Vasc Endovasc Surg. 2009; 37(1):46–55. doi: 10.1016/j.ejvs.2008.09.013 PMID: 19008128

22. Tieu BC, Lee C, Sun H, Lejeune W, Recinos A, Ju X, et al. An adventitial IL-6/MCP1 amplification loop accelerates macrophage-mediated vascular inflammation leading to aortic dissection in mice. J Clin Invest. 2009; 119(12):3637–3651. doi: 10.1172/JCI38308 PMID: 19920349

23. Xiong W, Zhao Y, Prall A, Greiner TC, Baxter BT. Key roles of CD4+ T cells and IFN-gamma in the development of abdominal aortic aneurysms in a murine model. J Immunol. 2004; 172(4):2607–2612. doi: 10.4049/jimmunol.172.4.2607 PMID: 14764734

24. Xiong W, MacTaggart J, Knispel R, Worth J, Persidsky Y, Baxter BT. Blocking TNF-alpha attenuates aneurysm formation in a murine model. J Immunol. 2009; 183(4):2741–2746. doi: 10.4049/jimmunol.0803164 PMID: 19620291

25. Elmore JR, Keister BF, Franklin DP, Youkey JR, Carey DJ. Expression of matrix metalloproteinases and TIMPs in human abdominal aortic aneurysms. Ann Vasc Surg. 1998; 12(3):221–228. doi: 10.1007/s100169900144 PMID: 9588507

26. Hasan D, Chalouhi N, Jabbour P, Hashimoto T. Macrophage imbalance (M1 vs. M2) and upregulation of mast cells in wall of ruptured human cerebral aneurysms: preliminary results. J Neuroinflammation. 2012; 9:222. doi: 10.1186/1742-2094-9-222 PMID: 22999528

27. Vorp DA, Vande Geest JP. Biomechanical determinants of abdominal aortic aneurysm rupture. Arterioscler Thromb Vasc Biol. 2005; 25(8):1558–1566. doi: 10.1161/01.ATV.0000174129.77391.55 PMID: 16055757

28. Annabi B, Shedid D, Ghosn P, Kenigsberg RL, Desrosiers RR, Bojanowski MW, et al. Differential regulation of matrix metalloproteinase activities in abdominal aortic aneurysms. J Vasc Surg. 2002; 35(3):539–546. doi: 10.1067/mva.2002.121124 PMID: 11877705

29. Tian X, Fan J, Yu M, Zhao Y, Fang Y, Bai S, et al. Adipose stem cells promote smooth muscle cells to secrete elastin in rat abdominal aortic aneurysm. PLoS ONE. 2014; 9(9):e108105. doi: 10.1371/journal.pone.0108105 PMID: 25243605

30. Rahim SS, Khan N, Boddupalli CS, Hasnain SE, Mukhopadhyay S. Interleukin-10 (IL-10) mediated suppression of IL-12 production in RAW 264.7 cells also involves c-rel transcription factor. Immunology. 2005; 114(3):313–321. doi: 10.1111/j.1365-2567.2005.02107.x PMID: 15720433

31. Parameswaran N, Patial S. Tumor necrosis factor-alpha signaling in macrophages. Crit Rev Eukaryot Gene Expr. 2010; 20(2):87–103. doi: 10.1615/CritRevEukarGeneExpr.v20.i2.10 PMID: 21133840

32. Baer M, Dillner A, Schwartz RC, Sedon C, Nedospasov S, Johnson PF. Tumor necrosis factor alpha transcription in macrophages is attenuated by an autocrine factor that preferentially induces NF-kappaB p50. Mol Cell Biol. 1998; 18(10):5678–5689. doi: 10.1128/MCB.18.10.5678 PMID: 9742085

33. Teixeira LK, Fonseca BP, Vieira-de Abreu A, Barboza BA, Robbs BK, Bozza PT, et al. IFN-gamma production by CD8+ T cells depends on NFAT1 transcription factor and regulates Th differentiation. J Immunol. 2005; 175(9):5931–5939. doi: 10.4049/jimmunol.175.9.5931 PMID: 16237086

34. Patel MI, Melrose J, Ghosh P, Appleberg M. Increased synthesis of matrix metalloproteinases by aortic smooth muscle cells is implicated in the etiopathogenesis of abdominal aortic aneurysms. J Vasc Surg. 1996; 24(1):82–92. doi: 10.1016/S0741-5214(96)70148-9 PMID: 8691532

35. Galle C, Schandene L, Stordeur P, Peignois Y, Ferreira J, Wautrecht JC, et al. Predominance of type 1 CD4+ T cells in human abdominal aortic aneurysm. Clin Exp Immunol. 2005; 142(3):519–527. doi: 10.1111/j.1365-2249.2005.02938.x PMID: 16297165

36. Maiellaro K, Taylor WR. The role of the adventitia in vascular inflammation. Cardiovasc Res. 2007; 75(4):640–648. doi: 10.1016/j.cardiores.2007.06.023 PMID: 17662969

37. Majesky MW, Dong XR, Hoglund V, Mahoney WM, Daum G. The adventitia: a dynamic interface containing resident progenitor cells. Arterioscler Thromb Vasc Biol. 2011; 31(7):1530–1539. doi: 10.1161/ATVBAHA.110.221549 PMID: 21677296

38. Kim Y, Friedman A. Interaction of tumor with its micro-environment: A mathematical model. Bull Math Biol. 2010; 72(5):1029–1068. doi: 10.1007/s11538-009-9481-z PMID: 19908100

39. Yokoyama U, Ishiwata R, Jin MH, Kato Y, Suzuki O, et al. Inhibition of EP4 signaling attenuates aortic aneurysm formation. PLoS ONE. 2012; 7(5):e36724. doi: 10.1371/journal.pone.0036724 PMID: 22570740

40. Hao W, Friedman A. The LDL-HDL profile determines the risk of atherosclerosis: a mathematical model. PLoS ONE. 2014; 9(3):e90497. doi: 10.1371/journal.pone.0090497 PMID: 24621857

41. Raghavan ML, Vorp DA. Toward a biomechanical tool to evaluate rupture potential of abdominal aortic aneurysm: identification of a finite strain constitutive model and evaluation of its applicability. J Biomech. 2000; 33(4):475–482. doi: 10.1016/S0021-9290(99)00201-8 PMID: 10768396

42. Zelaya JE, Goenezen S, Dargon PT, Azarbal AF, Rugonyi S. Improving the efficiency of abdominal aortic aneurysm wall stress computations. PLoS ONE. 2014; 9(7):e101353. doi: 10.1371/journal.pone.0101353 PMID: 25007052

43. Lu ZY, Brailly H, Wijdenes J, Bataille R, Rossi JF, Klein B. Measurement of whole body interleukin-6 (IL-6) production: prediction of the efficacy of anti-IL-6 treatments. Blood. 1995; 86(8):3123–3131. PMID: 7579407

44. Wang DH, Makaroun MS, Webster MW, Vorp DA. Effect of intraluminal thrombus on wall stress in patient-specific models of abdominal aortic aneurysm. J Vasc Surg. 2002; 36(3):598–604. doi: 10.1067/mva.2002.126087 PMID: 12218961

45. Sule AA, Hwang TH, Chin TJ. Very high central aortic systolic pressures in a young hypertensive patient on telmisartan: Is central aortic systolic pressure associated with white coat hypertension? Int J Angiol. 2010; 19(4):e132–134. doi: 10.1055/s-0031-1278384 PMID: 22479144

46. Friedman A, Hao W. A Mathematical Model of Atherosclerosis with Reverse Cholesterol Transport and Associated Risk Factors. Bull Math Biol. 2014;. doi: 10.1007/s11538-014-0010-3 PMID: 25205457

47. Hao W, Crouser ED, Friedman A. Mathematical model of sarcoidosis. Proc Natl Acad Sci USA. 2014;. doi: 10.1073/pnas.1417789111 PMID: 25349384

48. Hao W, Rovin BH, Friedman A. Mathematical model of renal interstitial fibrosis. Proc Natl Acad Sci USA. 2014; 111(39):14193–14198. doi: 10.1073/pnas.1413970111 PMID: 25225370